

Coordinated Subcellular Organization in Bacteria

By Sinyu Yang

A thesis submitted in partial fulfillment of the requirements to receive a Bachelor of Science with Honors (Cellular, Molecular, and Developmental Biology) from the school of Literature, Sciences, and the Arts at the University of Michigan

2022

Acknowledgements:

I would like to extend my most sincere thanks to Lisa Pulianmackal and Dr. Anthony Vecchiarelli. Without their help and guidance for the past 2 years, this project and thesis would not have been possible. They are especially patient and understanding as I navigated working in the lab and my undergraduate studies. Apart from their mentorship, they also performed many of the experiments in this project and helped its progress. In particular, Lisa made majority of the constructs used in this study and obtained most of the microscopy images used for data analysis in the results section. Additionally, many of the figures used in this paper were arranged by Lisa, with some processed with her assistance. I would like to thank both Dr. Vecchiarelli and Lisa for their guidance during the writing process.

Lastly, I would also like to thank other members of the Vecchiarelli lab, whose support and input for this project helped refined the ideas presented here.

Abstract

In eukaryotes, linear motor proteins are responsible intracellular organization and transport¹. In prokaryotes, which do not have linear motors, the ParA/MinD (A/D) family of ATPases position and organize many genetic and protein-based cellular cargos²⁻⁴. ParA is well known for its role in the positioning of plasmid and chromosome segregation. MinD is known for its role in divisome positioning. Less studied are the A/D ATPases that position diverse protein-based organelles, such as Bacterial Microcompartments (BMCs)⁵⁻¹¹, flagella¹²⁻¹⁶, chemotaxis clusters¹⁷⁻²⁰, and conjugation machinery²¹. These systems have been previously studied independently to various degrees in different organisms, but never in the same cell. The question remains: can multiple A/D ATPases coexist and function to position disparate cargos? The Vecchiarelli group recently found that over a third of sequenced bacteria encode for multiple A/D ATPases (Pulianmackal et. al, in prep), and identified the model organism used in this study, *Halothiobacillus neapolitanus*, that encodes seven A/D ATPases for seven putative cellular cargos: chromosome, divisome, carboxysome BMC, flagellum, chemotaxis cluster, conjugation machinery, and nitrogen metabolism machinery. We used genetics and cell biology to show each A/D ATPase is responsible for the positioning of their respective cargos and created a strain of *H. neapolitanus* where multiple cargos are fluorescently labeled. The strain will serve as a useful tool to study the coordination of cargo positioning over the cell cycle.

Table of Contents

Acknowledgements:	1
Abstract	2
Introduction	4
Results	7
Section 1	7
Section 2	10
Section 3	12
Section 4	15
Section 5	17
Section 6	19
Section 7	21
Discussion	27
Methods	29
Bibliography	33

Introduction

In eukaryotic cells, motor proteins, actin filaments, and microtubules are well-known to be responsible for intracellular cargo transport and organelle organization. In bacteria, linear motor proteins are absent. Instead, a family of ParA/MinD (A/D) ATPases are responsible for the positioning of various cargos within the cell. These cargos include plasmids, chromosome^{21,22}, divisome²³, Bacterial Microcompartments (BMCs)⁵⁻¹¹, flagella¹²⁻¹⁶, chemotaxis clusters¹⁷⁻²⁰, and conjugation machinery²⁴. These systems have all been studied independently to varying degrees in model organisms that encode for few A/D ATPases. For example, *E. coli* only has a MinD for divisome positioning. *Caulobacter crescentus* has ParA-like proteins for both chromosome segregation and divisome positioning. *Bacillus subtilis* has a ParA for chromosome segregation, a MinD for divisome positioning, and FlhG for flagella positioning.

Although these A/D ATPases have been studied independently in different organisms, it is unclear how multiple A/D ATPases can coexist to position disparate cargos in the same cell. To investigate the prevalence of A/D ATPases in bacteria, the Vecchiarelli group used (PSI)-BLAST analysis with the chromosome segregation ParA from *Bacillus subtilis*, Soj, as a query. They found that ~ 95% of bacteria from the NCBI Reference Sequence database encode for at least one A/D ATPase and over a third encode for multiple A/D ATPases in the same cell (Pulianmackal et. al, in prep). At the top of the list was *Halothiobacillus neapolitanus* (*H. neapolitanus*) with seven putative A/D ATPases.

To determine if each A/D ATPase identified in *H. neapolitanus* is responsible for the positioning of disparate cargos, Pulianmackal and researchers performed gene neighborhood analysis. In bacteria, genes with associated functions are often arranged in operons, and A/D ATPase genes are often encoded near cargo-associated loci. For example, the ParAB

chromosome segregation system is typically encoded near the origin of replication (*OriC*). By analyzing the neighboring genes both upstream and downstream of the putative A/D ATPases, the Vecchiarelli lab identified the putative cargos of each A/D ATPase in *H. neapolitanus*: chromosome, divisome, carboxysome BMC, flagellum, chemotaxis cluster, conjugation machinery, and nitrogen metabolism machinery (**Figure 1**).

Here, we set out to experimentally identify the role of each A/D ATPase in positioning the cargo implicated by bioinformatics in *H. neapolitanus*. We use the model organism *H. neapolitanus* because of its experimental tractability. It also encodes for several A/D ATPases, which makes it a valuable tool for studying the mechanistic commonality and variation in the most widespread ATPase family used for the spatial organization of various cargos across prokaryotes. We use genetics and cell biology to directly link five of the putative A/D ATPases in *H. neapolitanus* to their respective cargos. Our findings show each ATPase is dedicated to the positioning and distribution of a specific cargo type. With this knowledge, we next created a strain in *H. neapolitanus* that has multiple cargos labeled with fluorescence protein in the same cell, which serves as a useful tool to further explore relative cargo positioning over the cell cycle. Taken together, our findings indicate that multiple A/D ATPases can coexist and function to position various cargos in the same cell.

Figure 1


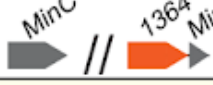
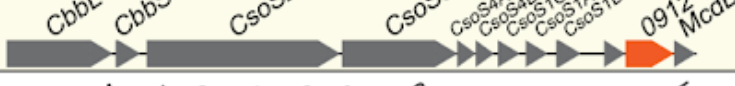


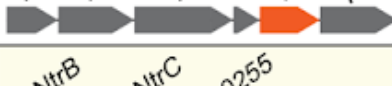

Gene name /number	Operon structure	Putative cargo
Hn2335		Chromosome
Hn1364		Divisome
Hn0912		Carboxysome
Hn0716		Flagella
Hn0722		Chemotaxis clusters
Hn1669		Conjugation machinery
Hn0255		Nitrogen metabolism

Figure 1: *Halothiobacillus neapolitanus* encodes seven ParA/MinD family ATPases. Gene neighborhood analysis identified the putative cargos of each putative ParA/MinD ATPase. (Accession numbers: Hn2335 - [ACX97145.1](#); Hn1364 - [ACX96198.1](#); Hn0912 - [ACX95755.1](#); Hn0716 - [ACX95565.1](#); Hn0722 - [ACX95571.1](#); Hn1669 - [ACX96495.1](#); Hn0255 - [ACX95118.1](#)) Unannotated ORFs on the table were annotated as “hypothetical proteins” in the genome.

Results

*All microscopy images shown in sections 1-5 were done by Lisa Pulianmackal

Section 1: The ParAB system segregates and positions chromosomes in *H. neapolitanus*

During cell division, it is critical that replicated chromosomes undergo segregation to ensure that both daughter cells inherit a copy. Chromosome mis-segregation produces non-viable anucleate cells. To ensure proper chromosome segregation and inheritance, most bacteria have the two-protein ParAB system to mediate this process. This system is typically encoded near the origin of replication (*OriC*), and the ParB protein binds to *parS*, a centromere-like site near *OriC*. ParB loads onto and around the *parS* site, forming a massive nucleoprotein complex that is the first point to segregate following chromosome replication²⁵. As such, fluorescently tagged ParB serves as a great marker for clear visualization of chromosome segregation and inheritance over the bacterial cell cycle.

We identified a putative *parA* (*Hn2335*) encoded near *OriC* in our model organism *H. neapolitanus*. Its genetic proximity to *OriC* suggests it is the ParA ATPase responsible for chromosome segregation. We tagged the ParB homolog downstream of *Hn2335* with the fluorescent protein monomeric Neon Green (mNG) to use it as a marker for chromosome segregation (**Figure 2A**). In short cells, ParB-mNG was observed as a single focus at mid-cell, while in longer cells ParB formed two foci at the quarter positions (**Figure 2B**). Population analysis confirmed this observation (**Figure 2B bottom**). When the putative *parA* gene (*Hn2335*) was deleted, ParB-mNG foci were randomly positioned in the cell (**Figure 2C**). Additionally, 25% of the $\Delta Hn2335$ deletion cell population had no foci (**Figure 2D**). For cells still harboring ParB foci, their fluorescence intensity was significantly brighter compared to ParB foci in WT cells (**Figure 2E**). These data suggest that the gene *Hn2335* is necessary for the positioning and segregation of ParB-mNG foci.

We next observed chromosome segregation in real-time using both ParB-mNG foci and SYTOX-staining of the nucleoid. In WT, newborn cells had a single ParB focus at mid-cell that bidirectionally split into two foci that moved to the quarter positions (**Figure 2F**). After division, these quarter positions become mid-cell in the daughters, thus ensuring faithful chromosome inheritance. This sequence of events was lost when the putative *parA* gene (*Hn2335*) was deleted, with unequal segregation of chromosomes producing some polyploid cells that continued to divide, and some anucleate cells that did not (**Figure 2G**). In addition, the unequal distribution of chromosomes after division resulted in anucleate daughter cells and daughter cells with increased ParB foci fluorescence intensities, which likely represent multiple chromosome copies being inherited in these cells (**Figure 2E**).

There were some variations of chromosome mispositioning and segregation observed in the $\Delta Hn2335$ deletion mutant population. While most cells had a single punctate ParB focus on the polar end of the cell that could not split, some mutant cells had ParB foci segregate and diffuse into opposing cell halves, thus allowing both daughter cell to inherit a copy after division (**Figure 2G**). Some cells had ParB foci transiently split but remained on the same side of the cell, producing a polyploid daughter cell and an anucleate daughter cell. The defects in chromosome segregation and inheritance resulted in a greater variation in cell length (**Figure 2H**). Taken together, the *Hn2335* gene identified as an A/D ATPase is required for the positioning and segregation of chromosomes (**Figure 2I**) and will hereby be designated as the protein ParA.

Figure 2

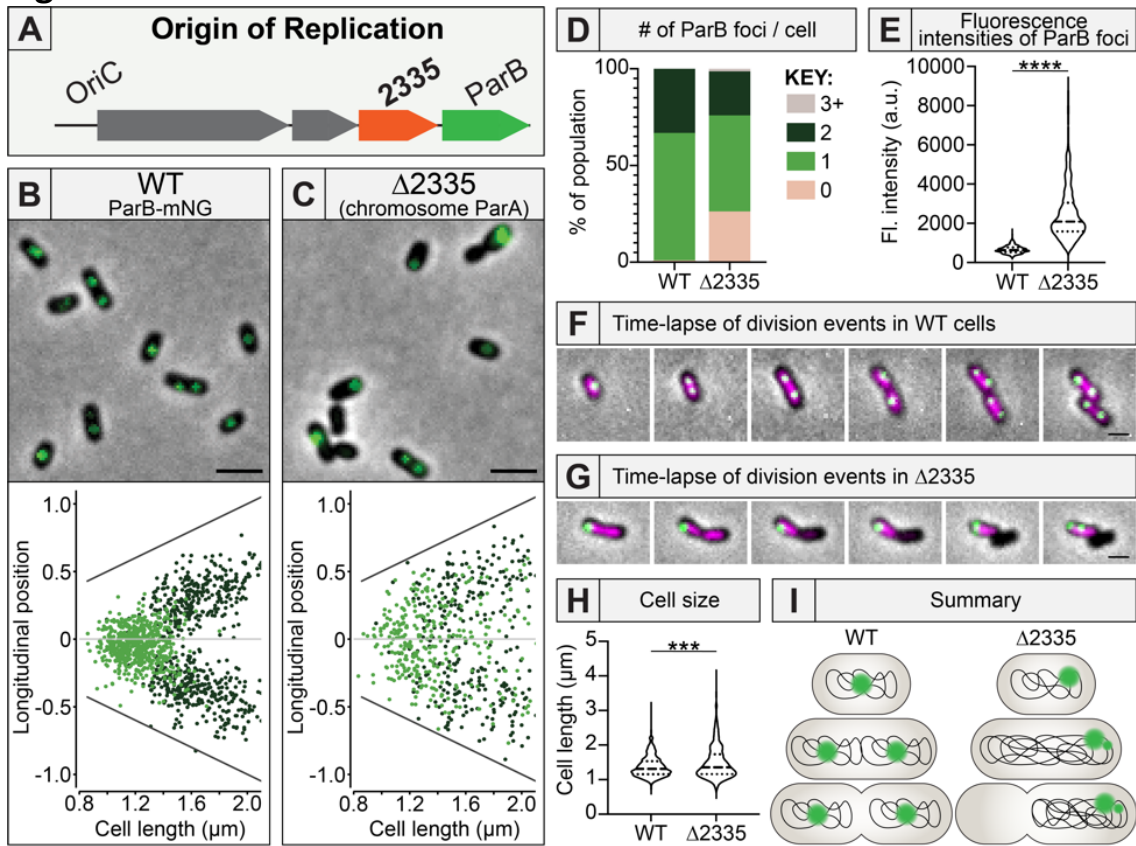


Figure 2: Gene 2335 encodes for ParA required for chromosome segregation in *H. neapolitanus*. (A) Gene 2335 is found near the origin of replication (*OriC*) and has a ParB-homolog encoded immediately downstream. The genomic location of *gene 2335* suggests it encodes for the chromosome segregation ParA ATPase. (B) Population analysis of foci localization: Cells were analyzed and quantified using MicrobeJ. On the x-axis, cells are organized according to increasing cell length. The foci on the graphs represent where the foci are found along the length of the cell. Light green: 1 focus/cell; dark green: 2 foci/cell. Mid-cell is denoted by a longitudinal position of 0. Short WT cells had a single ParB focus at mid-cell, whereas longer cells had two foci at the quarter positions. Scale bar: 2 μm (C) Δ2335 mutant cells displayed random positioning of ParB foci regardless of cell length. Scale bar: 2 μm (D) WT cells had 1-2 foci. 25% of Δ2335 cells had no foci. (E) Δ2335 cells had much brighter ParB foci compared to WT. Wilcoxon test p-value < 0.0001 (F) Newborn WT cells have a single ParB focus at midcell. Foci are then faithfully segregated to the quarter positions prior to division. Green: ParB foci; Magenta: SytoxBlue stain. Scale bar: 1 μm (G) In Δ2335, faithful foci positioning and segregation is lost. Because both ParB foci remain on the left hand side of the dividing cell, the cell on the right becomes anucleate following cell division. Green: ParB foci; Magenta: SytoxBlue stain. Scale bar: 1 μm (H) Δ2335 mutant cells displayed greater variability in cell size. Wilcoxon test p-value = 0.0006 (I) Gene 2335 is critical for chromosome segregation in *H. neapolitanus*.

Section 2: The MinCDE system positions the divisome for mid-cell division in *H. neapolitanus*

Positioning the divisome at mid-cell is required to produce daughter cells of roughly the same length. Many bacteria use the MinCDE system to position the cell division machinery at mid-cell. MinD is a ParA/MinD family ATPase, and when deleted, these mutant cells can asymmetrically divide at the nucleoid-free polar regions of the cell and produce anucleate “mini-cells”²⁶. Our bioinformatic analysis identified a MinD homolog, encoded by gene *Hn1364*. In the same operon immediately downstream of this gene is a MinE homolog. A MinC homolog is also identified in another location in the *H. neapolitanus* genome (**Figure 3A**). The presence of the MinCDE system suggests a role in divisome positioning in *H. neapolitanus*.

To determine the role of gene *Hn1364* in divisome positioning, we identified the constriction sites of dividing cells relative to their cell length (**Figure 3B, C**). In WT cells, constriction sites are localized to mid-cell (**Figure 3B, D**), while in cells deleted for *Hn1364*, the constriction sites are more randomly positioned throughout the cell (**Figure 3C, E**). Cell population analysis showed that 97% of constriction sites in WT cells were located at mid-cell compared to 41% in mutant cells (**Figure 3F**). In addition, cells deleted for *Hn1364* were more likely to divide asymmetrically, which resulted in a wider variation in cell length (**Figure 3E, H**). Mutant cells were also more likely to have multiple constriction sites in the same cell, with 9% of dividing cells having multiple simultaneous division sites along the cell length (**Figure 2G**). Altogether, our data show that gene *Hn1364* plays an important role in the mid-cell positioning of the *H. neapolitanus* divisome (**Figure 3I**), and hereby assign the protein as MinD.

Figure 3

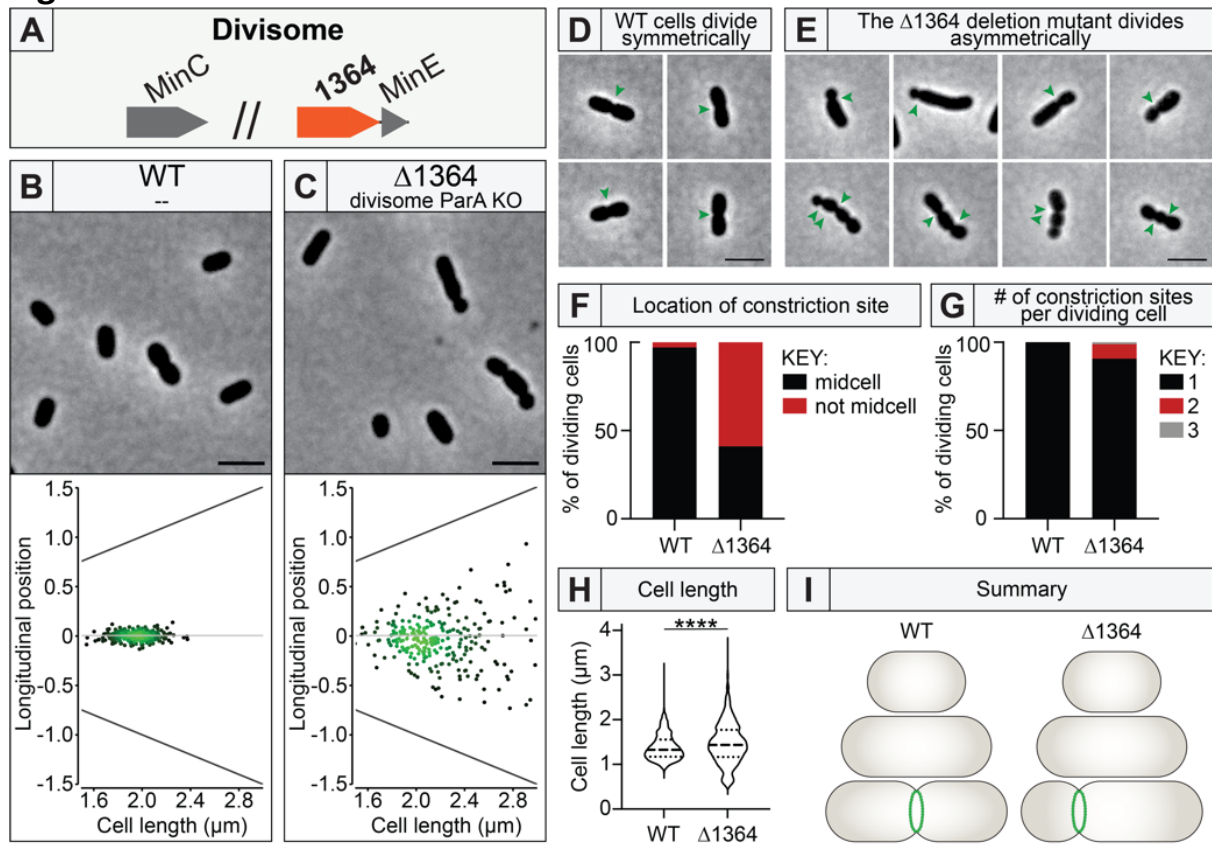


Figure 3: Gene 1364 encodes for MinD required for cell division positioning. (A) Gene 1364 is found directly upstream of *minE*. MinC is also present elsewhere in the genome. Therefore, the MinCDE system is present and likely involved in divisome positioning in *H. neapolitanus*. (B,C) Divisome positioning was determined by the location of constriction sites. For each mutant, ~300 dividing cells were analyzed for the location of their constriction sites relative to mid-cell. Each dot on the graph represents one identified constriction site. The center horizontal line represents mid-cell. In this density plot, light green represents high density and dark green represents low density. In WT cells, constriction sites were found close to mid-cell. In $\Delta 1364$, constriction sites could be found throughout the length of the cell. Scale bar: 2 μm (D) WT cells had constriction sites at mid-cell (green arrows). Scale bar: 2 μm (E) $\Delta 1364$ cells were more likely to divide asymmetrically at non-midcell locations (green arrows). Multiple division sites could also be found simultaneously on the same cell. Scale bar: 2 μm (F) 97% of WT cells divided at mid-cell. Only 41% of $\Delta 1364$ cells divided at mid-cell. Constriction sites were considered mid-cell when they were found within 5% of the cell center along the long axis. (G) WT cells only had one division site per cell at any given time. In $\Delta 1364$, 9% of dividing cells had multiple division sites per cell. (H) Mutant cells displayed greater variability in cell size. Wilcoxon test p-value < 0.0001 (I) Gene 1364 is critical for positioning the divisome at mid-cell in *H. neapolitanus*.

Section 3: The McdAB system encoded in the carboxysome operon is responsible for its positioning

In bacteria, bacterial microcompartments, or BMCs, play an important role in carbon fixation and utilization of carbon sources, and therefore have great ecological, medical, and biotechnological interest. BMCs are prevalent across bacteria, with BMCs found in 29 bacterial phyla and about 20% of sequenced bacterial genomes²⁷. The model BMC is the carbon-fixing carboxysome found in cyanobacteria and proteobacteria^{6,28}. Carboxysomes encapsulate and enrich RuBisCo with its CO₂ substrate to increase its enzymatic efficiency. Despite their importance and prevalence across the bacterial world, how BMCs are spatially regulated remains relatively unstudied. Recently, our lab found that an A/D ATPase, which we termed Maintenance of carboxysome distribution protein A (McdA), is required for the distribution and positioning of carboxysomes along the nucleoid of cells, and it functions along with a partner protein called McdB^{5,8,10}. We found that this McdAB system is conserved in carboxysome-containing proteobacteria, including our key model organism in the study of carboxysome structure and function, *H. neapolitanus*^{11,28}.

Gene *Hn0912* is the A/D ATPase found near the carboxysome operon and identified as McdA (**Figure 4A**). Its genetic location near genes encoding carboxysome shell proteins and RuBisCo suggests its role in carboxysome distribution and positioning in the cell. To verify its involvement, we performed fluorescence microscopy and visualized carboxysomes by tagging the encapsulated Rubisco enzyme in *H. neapolitanus*, CbbS, with mTurquoise2. In WT cells, carboxysome foci were equally distributed down the cell length (**Figure 4B**). In the $\Delta Hn0912$ mutant, carboxysomes were no longer distributed. Rather, carboxysomes formed a massive aggregate that localized to the poles. (**Figure 4C**).

The mutant also had fewer foci per cell compared to that of WT cells. In the WT population, 95% of cells had 3 or more carboxysome foci, while in the mutant population, only 5% of cells have 3 or more foci (**Figure 4D**). Most mutant cells only had 1 or 2 massive aggregates at one or both cell poles. In addition, although mutant cells had fewer carboxysome foci, the massive aggregate foci were much brighter compared to the fluorescence intensity of distributed carboxysomes in WT cells (**Figure 4E**). Taken together, the decrease in foci number and increase in fluorescence intensity of foci are consistent with our previous TEM data showing that fully assembled carboxysomes aggregate at the poles in the absence of a functional McdAB system ²⁹

To visualize carboxysome dynamics in real time, time-lapse microscopy was performed. In WT cells, carboxysomes were dynamically positioned throughout the cell cycle and across generations (**Figure 4F**). In mutant cells, carboxysomes were stagnant throughout cell growth and division across several generations (**Figure 4G**). Our findings here provide further evidence showing that the A/D ATPase in the carboxysome operon is responsible distributing carboxysomes. We already designated this protein as McdA (**Figure 4H**).

Figure 4

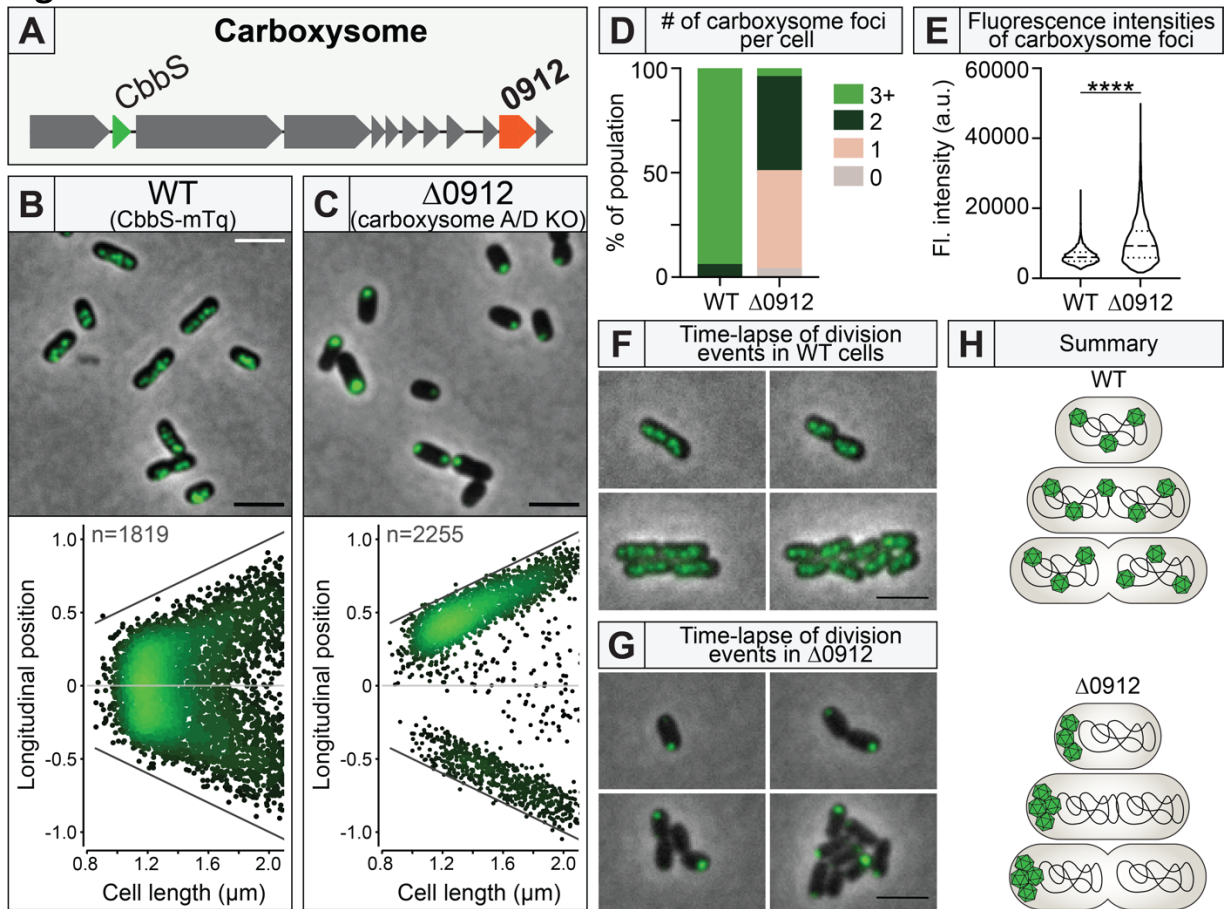


Figure 4: Carboxysome positioning is determined by McdA, the Para/MinD-like ATPase encoded in the carboxysome operon. (A) Gene *0912* encodes McdA and is found near genes encoding carboxysome shell proteins and RuBisCO. **(B)** Population analysis of foci localization: Cells were analyzed and quantified using MicrobeJ. On the x-axis, cells are organized according to increasing cell length. The foci on the graphs represent where the foci are found along the length of the cell. In WT cells, carboxysomes are distributed across the cell length. Scale bar: 2 μm **(C)** In $\Delta mcdA$ mutant cells, carboxysomes formed a large polar focus at one or both poles. Scale bar: 2 μm **(D)** 95% of WT cells had 3+ carboxysome foci. Only 5% of $\Delta mcdA$ cells had 3+ foci. **(E)** $\Delta mcdA$ cells had much brighter carboxysome foci compared to WT. Wilcoxon test p-value < 0.0001 **(F)** In WT, carboxysomes are dynamically positioned along the cell length throughout the cell cycle and across multiple generations. Scale bar: 2 μm **(G)** In $\Delta mcdA$, carboxysome aggregates were stagnant throughout the cell cycle and across multiple generations. Scale bar: 2 μm **(H)** Cell size. Wilcoxon test p-value **(I)** Gene *0912* encodes for McdA, which is essential for carboxysome distribution and inheritance following cell division.

Section 4: In *H. neapolitanus*, flagella number and positioning are regulated by gene *Hn0716*

Flagella are external filamentous structures that allow for bacterial motility. Flagella location, number, and pattern vary across different bacteria. *E. coli* flagellation patterns occur randomly³⁰, while others rely on markers at the cell pole, such as the case of the Tip system of *C. crescentus*^{31,32}. Many bacteria have an A/D ATPase encoded in their flagellar operon, *flhG*, which is crucial for flagellation patterns^{12,15,16,33–35}. However, the mechanism remains unclear. Previous studies show that deletion of *flhG* affects flagellar position, number, and pattern. Our bioinformatic analysis suggests that in *H. neapolitanus*, gene *Hn0716* encodes an FlhG homolog within the flagella operon (**Figure 5A**).

To study if gene *Hn0716* plays a role in the positioning of flagella, we created a fusion protein of mNG-FliN, which allows us to visualize the flagella machinery. FliN is a component of the flagellar basal body that assembles on the cytoplasmic side of the membrane (**Figure 5A**)³⁶. In WT cells, we observed a singular mNG-FliN focus on the pole (**Figure 5B**). In *Hn0716* deleted mutants, FliN foci were no longer only faithfully localized to one pole. Instead, foci were more randomly distributed (**Figure 5C**). Also, most WT cells only had one focus, while mutant cells were 3.5 times more likely to have two or more foci, and 2.5 times more likely to have no foci at all (**Figure 5D**). Fluorescence intensity analysis showed that even when mutant cells had foci, their intensity was much lower than WT (**Figure 5E**).

Next, we determined if this mispositioning of FliN affected cell mobility. Mobility assays show that *Hn0716* deletion cells were not motile (**Figure 5F**). This loss in mobility could be due to mispositioning of flagella, a loss of flagella, or hyper-flagellation. To visualize flagella, we made flagellin^{T185C}, which allows flagella to be fluorescently stained by adding a cysteine-reactive maleimide stain to the media. Imaging results showed that WT cells are monotrichous,

with a single flagellum at the same pole as the FliN focus (**Figure 5G left**). In *Hn0716* deleted cells, flagella are still observed at the same pole as FliN foci, but the cells often have multiple flagella, with many of them malformed and bundled together (**Figure 5G right**). All data above suggest that gene *Hn0716* is important for regulating the number and position of flagella in *H. neapolitanus*, and we hereby designate this protein as FlhG.

Figure 5

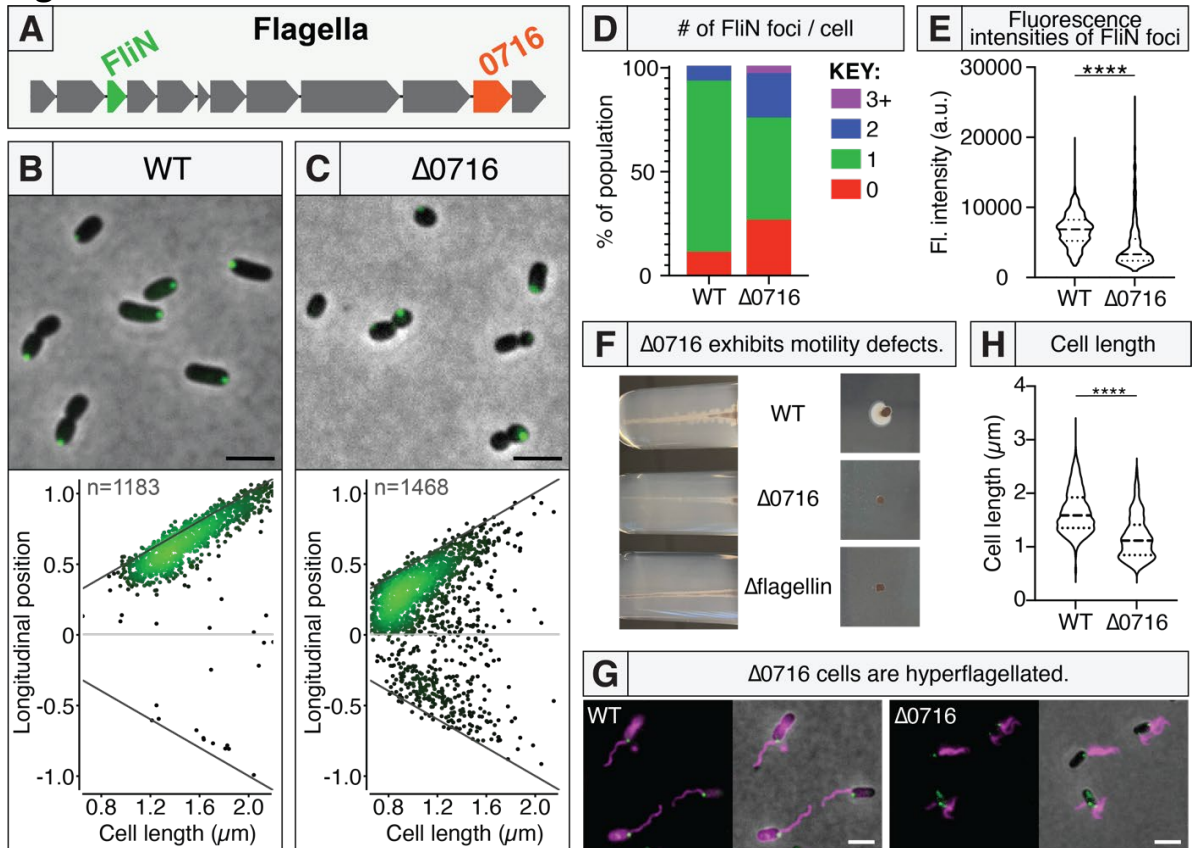


Figure 5: Gene 0716 encodes for FlhG required for regulating flagella position and copy number.

(A) Gene *0716* is found near flagella-associated genes, suggesting it is involved in positioning flagella. **(B)** Population analysis of foci localization: Cells were analyzed and quantified using MicrobeJ. On the x-axis, cells are organized according to increasing cell length. The foci on the graphs represent where the foci are found along the length of the cell. Cells were normalized for polarity of FliN foci; the pole of the cell that is closest to the FliN focus is oriented to the top. Foci under the mid-cell mark represent a second focus in the cell. WT cells had a single polar FliN focus. Scale bar: 2 μm **(C)** In $\Delta 0716$ cells, FliN foci were more randomly positioned along the cell length. Scale bar: 2 μm **(D)** 85% of WT cells had a single focus whereas only 45% of $\Delta 0716$ cells had a single focus. $\Delta 0716$ cells were more likely to have additional foci. **(E)** When FliN foci were present in $\Delta 0716$ cells, the foci were much dimmer than those of WT cells. Wilcoxon test p-value < 0.0001 **(F)** $\Delta 0716$ was not motile in motility assays. **(G)** WT cells had a single

polar flagellum next to the FlIN focus. $\Delta 0716$ cells typically had multiple flagella, sometimes found as tufts. Scale bar: 2 μm

Section 5: Positioning of chemotaxis cluster in *H. neapolitanus* is regulated by gene *Hn0722*

Chemotaxis clusters direct bacterial motility, and they are composed of large hexagonal arrays of chemoreceptors, with an adaptor protein (CheW), and a kinase (CheA). Bacteria use flagella to move toward favorable environments detected by chemotaxis. The inheritance of chemotaxis and flagella are crucial to ensure that cells can appropriately sense and respond to their environment, therefore, it is important that they are positioned and inherited by daughter cells to gain survival advantage. There are many evolved mechanisms to control the number and positioning of chemotaxis clusters, such as random self-assembly in *E. coli*³⁷, markers on cell-pole in *C. crescentus*³⁸, and the use of A/D ATPases in *Rhodobacter sphaeroides* and *Vibrio cholerae*, called ParC^{19,39}. With respect to the A/D ATPase system positioning chemotaxis clusters, previous studies have shown that the deletion of this system results in the mispositioning and reduction of chemotaxis clusters in the cell.

Our bioinformatics analysis showed that gene *Hn0722* encodes a protein that is a ParC homolog in the chemotaxis operon of *H. neapolitanus*. Within the operon, CheY is a protein that serves as a response regulator phosphorylated by CheA at the chemotaxis cluster. Studies have previously shown that CheY colocalizes with chemotaxis clusters in *E. coli*^{40,41}. Therefore, to study the role of *Hn0722* in the positioning of chemotaxis clusters, we used a CheY-mNG fusion protein as a marker (**Figure 6A**). We found that mNG-CheY forms a single polar focus in ~85% of WT cells (**Figure 6B**), which is consistent with electron micrographs of chemotaxis arrays previously described in *H. neapolitanus*⁴². In *Hn0722* deleted cells, ~80% of the mNG-CheY foci signal was diffuse (**Figure 6CD**). In addition, the remaining ~20% of mutant cells had mispositioned foci (**Figure 6C**), and significantly lower in intensity compared to WT (**Figure**

6E). Overall, the data suggest that the A/D ATPase encoded by gene *Hn0722* is important for positioning chemotaxis clusters in *H. neapolitanus* (**Figure 6F**) and will hereby refer to this protein as ParC.

Figure 6

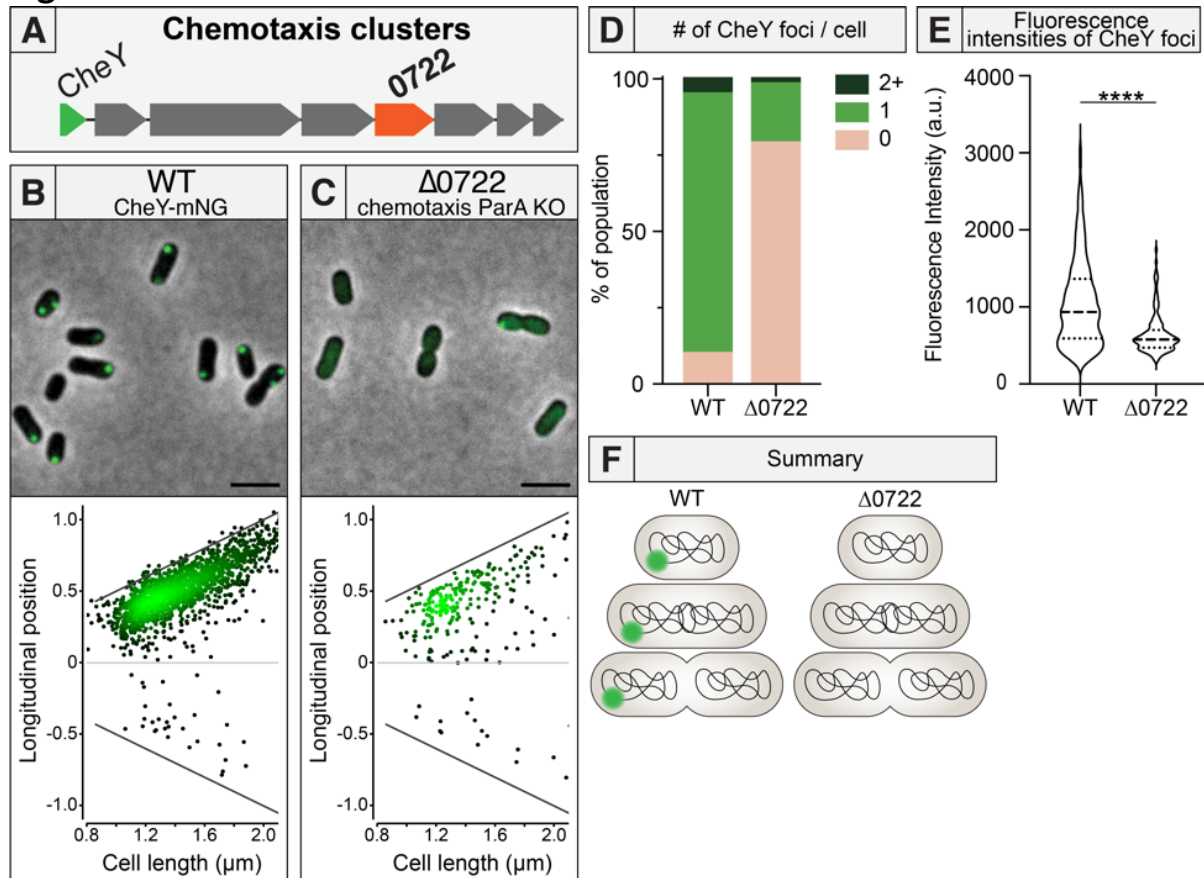


Figure 6: Gene 0722 encodes for ParC required for chemotaxis cluster positioning. (A) Gene 0722 is found near chemotaxis-associated genes, suggesting its involvement in positioning chemotaxis clusters. **(B)** Population analysis of foci localization: Cells were analyzed and quantified using MicrobeJ. On the x-axis, cells are organized according to increasing cell length. The foci on the graphs represent where the foci are found along the length of the cell. Cells were normalized for polarity of CheY foci; the pole of the cell that is closest to the CheY focus is oriented to the top. Foci under the mid-cell mark represent a second focus in the cell. WT cells had a single CheY polar focus. Scale bar: 2 μm **(C)** Δ0722 mutant cells typically had no CheY foci. Scale bar: 2 μm **(D)** 87% of WT cells had one focus whereas only 19% of Δ0722 cells had a single focus. **(E)** When Δ0722 cells did have a detectable focus, the foci were much dimmer in fluorescence intensity compared to WT. Wilcoxon test p-value < 0.0001 **(F)** Gene 0722 is critical for chemotaxis cluster assembly and positioning in *H. neapolitanus*.

Section 6: Complementation assay for each putative A/D ATPase restores WT phenotype

To confirm the role of each A/D ATPase in the positioning of their respective cargos, we performed complementation experiments for each cargo. Each putative A/D ATPase was put under a pTrc promoter and induced with pre-determined IPTG concentrations for controlled expression of protein. The pTrc-A/D ATPase constructs were transformed into the corresponding A/D ATPase knockout strains to observe complementation.

Complementation for each cargo was observed with different IPTG concentrations and incubation periods. The *parA* deletion mutant saw *parB*-mNG foci localized to the pole rather than the mid-cell or quarter position observed in WT (**Figure 7A left and middle**). pTrc-*parA* showed restoration of the WT phenotype with 50uM IPTG after 3 hours of incubation (**Figure 7A right**). Deletion of McdA show cells that form carboxysome aggregates at the pole, while WT cells have carboxysomes positioned and distributed throughout the cell length (**Figure 7B**). Complementation was observed with 50uM of IPTG after 3 hours of incubation. In *minD* deletion cells, we saw asymmetric cell division, rather than the mid-cell division seen in WT (**Figure 7C**). Δ *minD* cells transformed with pTrc-*minD* saw restoration of mid-cell division after incubation with 50uM IPTG for 6 hours. Deletion of *flhG* produced cells with atypical flagella number, location, and motility compared to WT cells (**Figure 7D**). Interestingly, complementation with pTrc-*flhG* in Δ *flhG* cells saw regulation of flagella number and location without IPTG induction. Leaky expression from the pTrc promoter was sufficient to restore WT phenotype (**Figure 7D**). Lastly, the complementation assay for chemotaxis clusters is still in progress (**Figure 7E**). Together, I restored the WT phenotype in complemented cells for 4 of the 5 cargos studied, strongly implicating the role of these A/D ATPases in the positioning and regulation of their respective cargos.

Figure 7

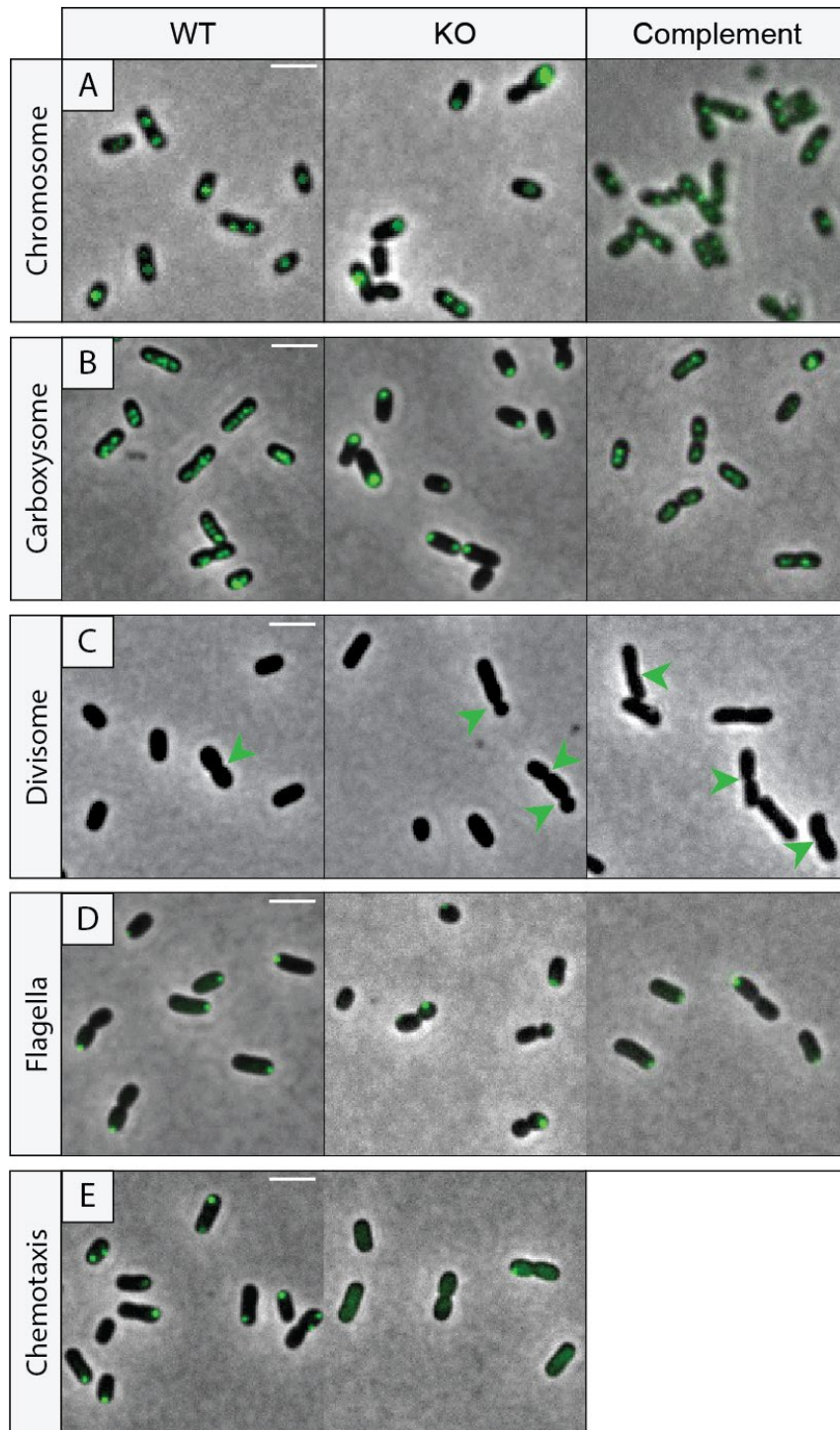


Figure 7: complementation assay shows restoration of WT phenotype

(A) ParB-mNG was used to visualize chromosome positioning. In short WT cells, chromosome foci are localized to the mid-cell, while in longer WT cells, they are localized to the quarter positions. In *parA* knockout (KO) cells, chromosome foci are randomly positioned regardless of cell length. In complemented cells, WT positioning of foci is restored. Scale bar: 2 μm . **(B)** CbbS-mTq was used to

visualize carboxysome distribution and positioning. In WT, carboxysomes are distributed along the length of the cell. In *mcdA* KO cells, carboxysomes were seen as aggregates that localize to the pole. In complemented cells, carboxysome distribution is restored. Scale bar: 2 μm . **(C)** Divisome positioning was determined by the location of constriction sites (green arrows). In WT cells, constriction sites were found close to midcell. In *minD* KO mutants, constriction sites were sporadically found throughout the cell length. In complemented cells, constriction sites are found again at the mid-cell. Scale bar: 2 μm . **(D)** mNG-FliN was used to visualize flagella focus. In WT cells, a single flagella focus is localized to the pole. In *flhG* KO cells, there were irregular number and positioning of flagella foci. In complemented cells, singular flagella focus localized to the pole was restored. Scale bar: 2 μm . **(E)** CheY-mNG was used to visualize chemotaxis clusters. In WT cells, a polar singular focus was observed. In *parC* KO cells, foci signal was diffused. Complementation for *parC* KO cells is still in progress. Scale bar: 2 μm .

Section 7: Strain with multiple labeled cargos to visualize the coordination of cargo positioning

In our experiments described above, we successfully visualized five cargos in *H. neapolitanus* individually. Thus far, ParB, FliN, and CheY have been labeled with mNG, while CbbS was labeled with mTQ, and we were able to observe divisome positioning via cell constriction sites from Phase Contrast microscopy. With individual cargos labeled, each could be visualized and studied independently in each cell, which allowed us to link A/D ATPases to their putative cargos and observed individual cargo positioning during the cell cycle. However, we have not been able to study how multiple A/D ATPases coordinate the positioning of numerous cargos at the same time in one cell. To study the dynamics and positioning of each cargo together throughout the cell cycle, we set out to label the cargos simultaneously in the same cell.

For visualization of all cargos at once with microscopy, we selected different colors that allowed for independent visualization for each fusion protein. The fluorescent proteins chosen had minimal overlap in excitation and emission wavelengths, limiting the non-specific background signal due to bleed through of the fluorescence microscope filters (**Figure 8**). This ensured that we could visualize each cargo foci distinct from each other. Earlier, we already created CheY-mNG to visualize chemotaxis clusters and CbbS-mTq to visualize carboxysome foci. We decided to label ParB with mScarlet to visualize chromosome foci, as it was reported to

be a very bright red protein ⁴³, and a Halotag stained with far-red dye was used to label FliN for visualization of the flagella focus. We did not use a far-red protein as most have excitation and emission spectrums that overlap with our red fluorescent protein mScarlet. I created fusion proteins to fluorescently label four cargos in *H. neapolitanus*: the chromosome origin region (ParB-mScarlet), the carboxysome (CbbS-mTQ), the chemotaxis cluster (CheY-mNG), and the flagellum (FliN-Halotag). The FliN-Halotag was visualized through staining with a far-red dye, JaneliaFluor650. The constriction sites remain the marker for divisome positioning.

Our initial multi-label strain allowed for visualization of multiple cargos in the same cell (**Figure 9**). Earlier, with single-label strains, we saw chromosome foci at the mid-cell, carboxysome foci distributed along the length, and chemotaxis and flagella foci at the poles. With multiple cargos labeled, we still see the same positioning for each cargo as we observe in the single label strains. Interestingly, now we see that the flagella and chemotaxis foci colocalize to the same pole in cells (**Figure 9**)! The data suggests a potential coordination between ParC and FlhG in their positioning of chemotaxis arrays and flagella, respectively. This will be a major question for future study.

Unfortunately, during long-term imaging, we noticed the ParB-mScarlet foci photobleached within 30 minutes at 10% SOLA power. The photostability of the fluorescent proteins is crucial for long term visualization of the foci. We replaced mScarlet with mApple, mCherry, and other red fluorescent proteins. Although mApple is not theoretically as stable or bright compared to the other two proteins, empirically it was the best candidate for long-term fluorescence microscopy in *H. neapolitanus* (**Figure 10**).

Still in progress is the optimization of the Halotag staining protocol in my strain with multiple labeled cargos. Currently, a staining protocol for Halotag in *H. neapolitanus* has not

been established. We are one of the first to attempt Halotag staining in this model organism, and our best conditions thus far were not optimal for time-lapse imaging, as the dye concentration was insufficient to stain the Halotag in newborn cells. Further optimization of incubation time, temperature, and dye concentration is needed to visualize the flagella foci in the multi-label strain across generations.

We have successfully visualized five cargos together in the same cell. Following optimization of the Halotag stain, this multi-label strain will be a useful tool to study the dynamic positioning of multiple cargos across generations. Additionally, it can also be a useful model to study the impact and effect of cargo mispositioning on other important cellular components in the cell.

Figure 8

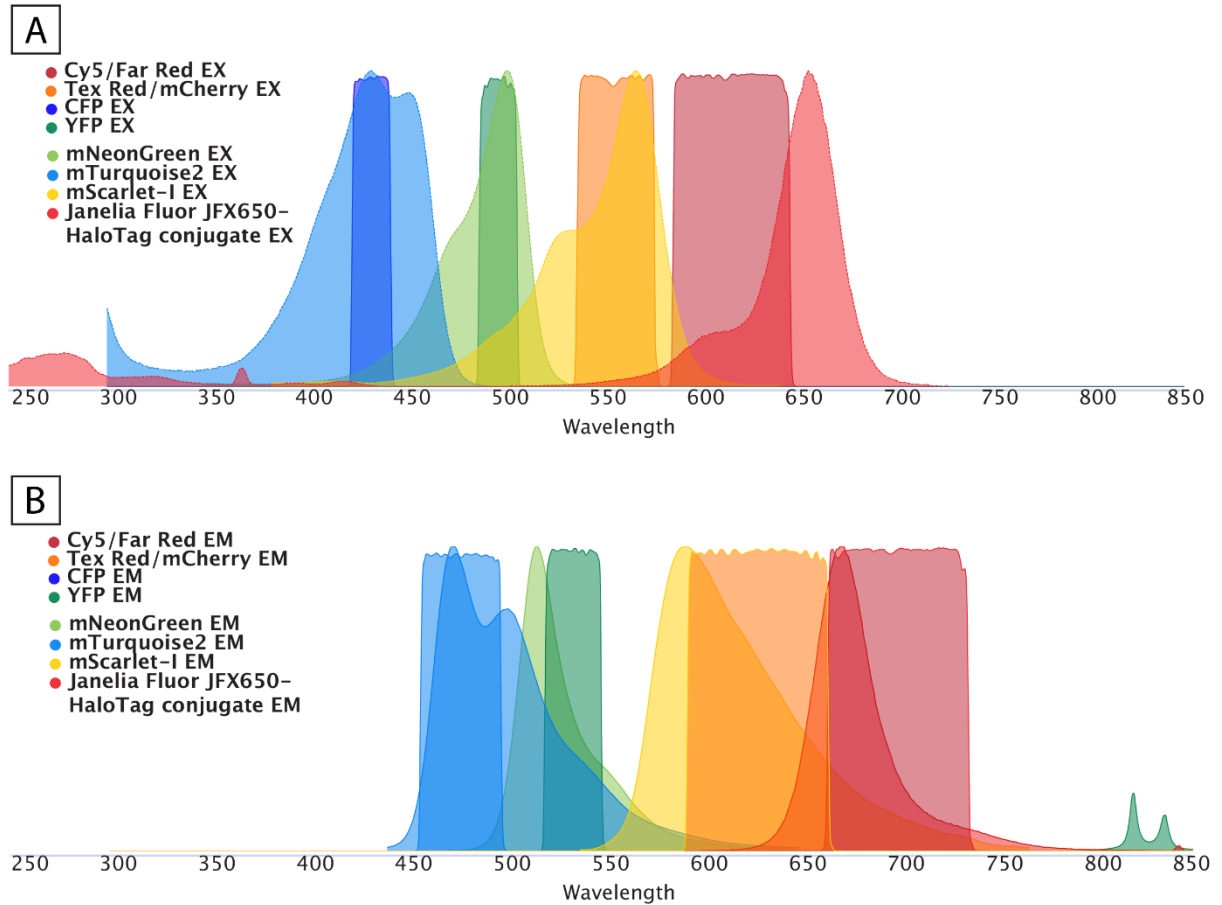


Figure 8: Fluorescent protein Excitation and Emission spectra

(A) The excitation spectra of the four fluorescent proteins selected to label multiple cargos in *H. neapolitanus* show different wavelengths (nm) with no significant overlap in peaks (Light blue, light green, light yellow, light red). The filter set used to visualize each fluorescent protein is shown in darker colors. The “Cy5/Far Red” filter set is used to image the Halotag stained with Janelia Fluor 650 dye. The “Tex Red/mCherry” filter set is used to image mScarlet-I. The “CFP” filter set is used to image mTq. The “YFP” filter set is used to image mNG. Source: FPbase **(B)** The emission spectrum for the four fluorescent proteins also shows no significant overlap in peaks (light blue, light green, light yellow, light red). The filter set used to visualize each fluorescent protein is shown in darker colors.

Figure 9

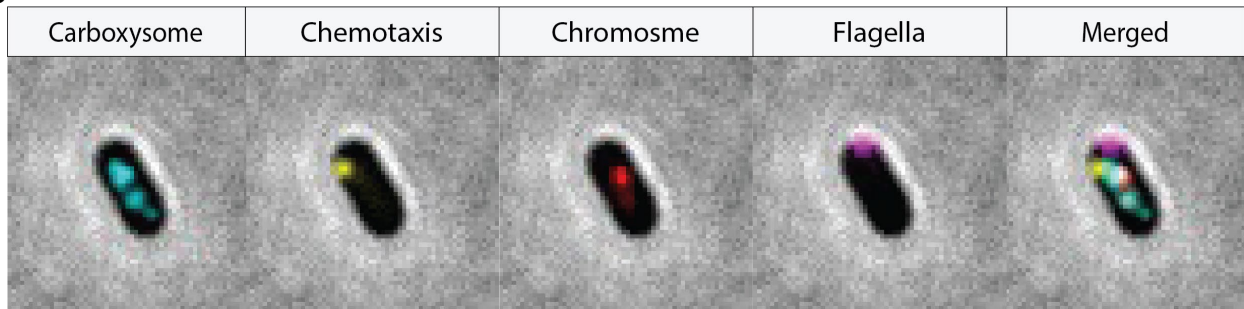


Figure 9: A strain of *H. neapolitanus* was created with multiple cargos labeled in the same cell. For each cargo, a fusion protein was created to tag the cargo with a fluorescent protein for visualization with fluorescent microscope. CbbS-mTq showed carboxysome foci distributed along the length of the cell, CheY-mNG showed chemotaxis focus positioned at the pole. ParB-mScarlet showed chromosome focus positioned at mid-cell. FliN-Halotag showed flagella focus positioned at the pole. Merged channels show all 4 cargos positioned in the same cell. CheY-mNG (yellow) is observed to be localized to the same pole as FliN-Halotag (purple).

Figure 10

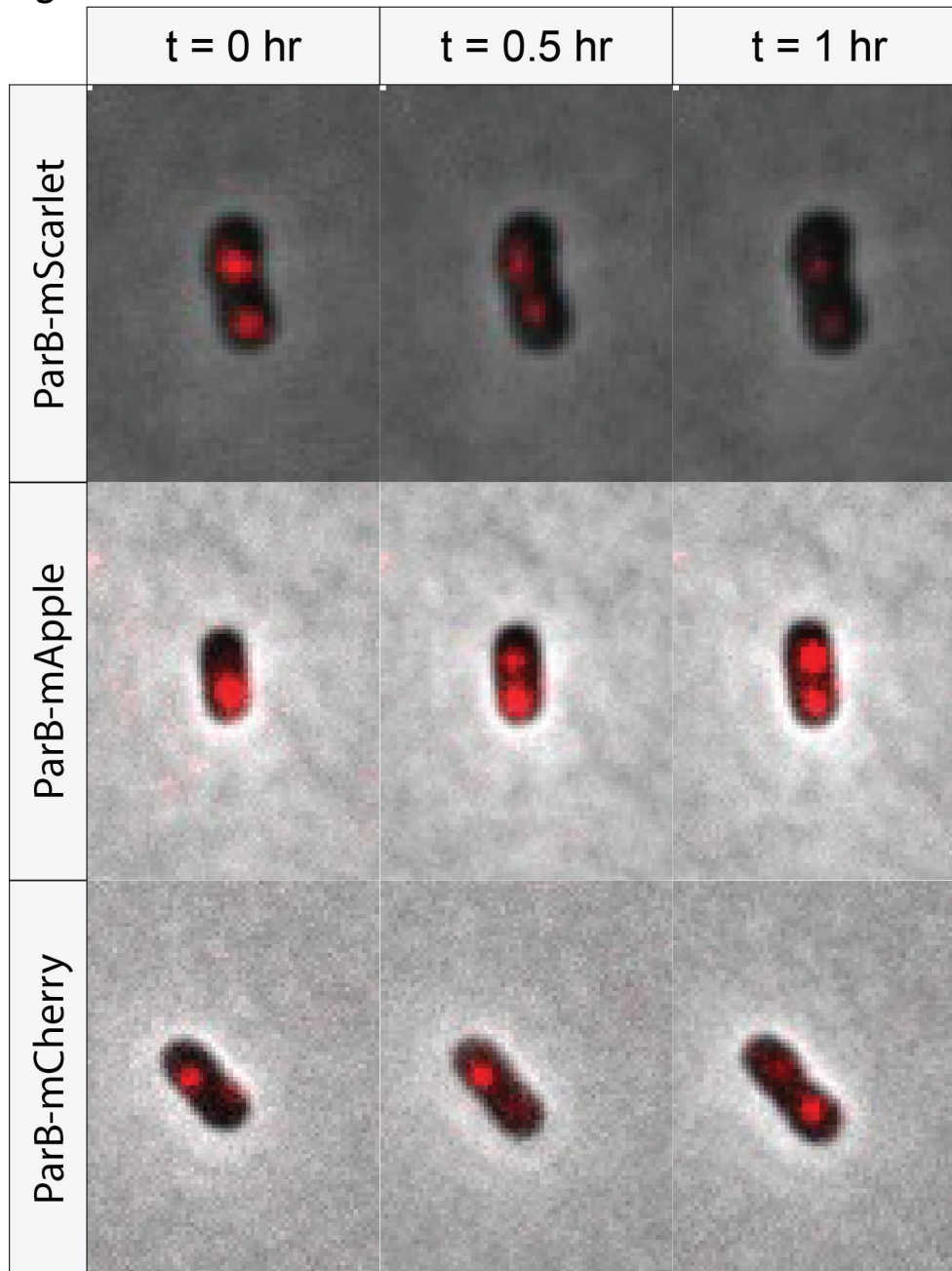


Figure 10: photostability comparison between mScarlet, mApple, and mCherry (IN PROGRESS)

(A) ParB-mScarlet was visualized at 10% SOLA power with 2 seconds of exposure time. After 30 minutes, the signal started to show bleaching. After an hour, the signal became significantly bleached. ParB-mApple was visualized at 5% SOLA power with 2 seconds of exposure time. The signal does not bleach and remain stable after an hour of imaging. ParB-mCherry was visualized at 5% SOLA power with 2 seconds of exposure time. The signal remains stable after an hour of imaging. However, the signal detected was significantly dimmer compared to mApple.

Discussion

Previously, the study of subcellular organization had been focused on specific biological processes and associated cellular cargos, rather than the focus being on their spatial positioning. A great example are BMCs, which has been studied since the 1950s, but the Vecchiarelli lab only recently discovered their A/D-based positioning system⁵⁻¹¹. Here, our focus was on spatial organization by the positioning systems, rather than a specific cargo. This is the first systems biology approach used to determine how multiple A/D ATPases coexist and position their respective cargos in the same cell.

The Vecchiarelli group had shown that over 95% of bacteria have at least one A/D ATPase, while over a third has multiple A/D ATPases and identified the organism *H. neapolitanus* that encodes for seven (Pulianmackal et. al, in prep). They had assigned each A/D ATPase with its putative cargo using gene neighborhood analysis. With genetics and cell biology techniques, we confirmed the role of each A/D ATPase in the regulation and positioning of their respective cargos in *H. neapolitanus*. We showed that multiple A/D ATPases can coexist and function in the same cell, and established *H. neapolitanus* as the model organism to study multiple A/D ATPases in one cell.

A future direction will be to use *H. neapolitanus* to determine the how positioning reactions by A/D ATPases are altered for different cargos. The study of A/D ATPases is important as they are responsible for the spatial organization of cargos that are essential for bacterial cell function: growth, DNA segregation, division, motility, and metabolism. The multiple cargo labeled strain can be a useful tool to further investigate the cargo positioning dynamics and the potential impact of mispositioning on other functions/cargos in the cell. In addition, many A/D ATPases have putative cargos that are involved in pathogenesis. It has been

previously identified that many human pathogens, such as *Vibrio*, *Clostridia*, *Burkholderia*, *Mycobacteria*, and *Pseudomonas* species all encode for four or more A/D ATPases. Identifying these A/D ATPases and understanding their mechanisms could create potential drug targets for treatments of antibiotic-resistant infections.

Lastly, the prevalence of A/D ATPase systems across prokaryotes suggest the broad application and impact of studying their mechanism. As minimal self-organizing systems are vital tools for synthetic biology⁴⁴, understanding the specificity determinants for positioning of each cargo allows for application of this knowledge in the design of positioning systems for both natural and synthetic cargos in bacteria. Many groups are now repurposing BMCs to produce fuels, therapeutics, and chemicals⁴⁵⁻⁴⁷. However, these synthetic BMCs assemble in heterologous hosts as aggregates, likely because they are not co-expressed with their positioning system. We aim to design Minimal Autonomous Positioning Systems (MAPS) based off the A/D ATPase positioning systems to serve as spatial regulators for natural or synthetic cargos across plethora of bacterial species.

Methods

tBLASTn analysis. tBLASTn analysis was done using a ParA/MinD consensus sequence, as a query against RefSeq Representative genomes database with max target sequences as 5000 and E value threshold at 0.0001. Sequences were filtered for those that shared sequence homology and had one of the identified putative cargo genes, confirmed using webFlaGs (<https://pubmed.ncbi.nlm.nih.gov/32956448/>). The consensus query was generated using COBOLT (<https://pubmed.ncbi.nlm.nih.gov/17332019/>).

FlaG analysis. A few representative genomes were selected to display gene neighborhood conservation. Identification of replication origins (OriC's) were performed using Ori-Finder (<https://bmcbioinformatics.biomedcentral.com/articles/10.1186/1471-2105-9-79>). FlaGs analysis figure was generated using Gene Graphics (<https://katlabs.cc/genegraphics/>).

Multiple sequence alignment. Sequences were aligned using Clustal Omega. The resulting tree was imported into iTOL to generate an unrooted tree.

Media and growth conditions. All mutants described in this study were constructed using WT *Halothiobacillus neapolitanus* (Parker) Kelly and Wood (ATCC® 23641™) purchased from ATCC. Cultures were grown in ATCC® Medium 290: S-6 medium for Thiobacilli (Hutchinson et al., 1965) and incubated at 30°C, while shaken at 130 RPM in air supplemented with 5% CO₂. Strains were preserved frozen at -80°C in 10% DMSO.

Construct designs and cloning. All constructs were generated using Gibson Assembly and verified by sequencing. Fragments for assembly were synthesized by PCR or ordered as a gBlock (IDT). Constructs contained flanking DNA that ranged from 750 to 1100 bp in length upstream and downstream of the targeted insertion site to promote homologous recombination into target genomic loci. Cloning of plasmids was performed in chemically competent *E. coli* Top10 or Stellar cells (Takara Bio).

Making competent cells in *H. neapolitanus* C2. Competent cells of *H. neapolitanus* were generated as previously reported. In short, 1 L of culture was grown to an OD of 0.8-0.15. Cultures were harvested by centrifugation at 5,000xg for 20 minutes at 4°C. Pellets were resuspended and washed twice with 0.5 volumes of ice-cold nanopore water. All wash centrifugation steps were performed at 3,000xg for 30 minutes at 4°C. The resulting pellet after washing was resuspended in 1x10⁻³ volumes of ice-cold nanopore water. These competent cells were used immediately or frozen at -80°C for future use. Frozen competent cells were thawed at 4°C before use.

Transformation in *H. neapolitanus* C2. 50-100 µL of competent cells were mixed with 5 µL plasmid DNA (1-5 µg) and incubated on ice for 5 minutes. This mixture is then transferred to a tube containing 5 mL ice-cold S6 medium without antibiotics and incubated on ice for 5 minutes. Transformations were recovered for 16-36 hours, shaken at 130 RPM, at 30°C, in air supplemented with 5% CO₂. Clones were selected by plating on selective medium with antibiotics. Colonies were restreaked. Restreaked colonies were verified for mutation by PCR.

Native fluorescent fusions. For the native fluorescent fusion of ParB-mNG, mNG-FliN, and CheY-mNG, the sequence encoding the fluorescent protein mNeonGreen (mNG) was attached to the 3' or 5' region of the native coding sequences, separated by a GSGSGS linker. For the native fluorescent fusion of Cbbs-mTq, the sequence encoding the fluorescent protein mTurquoise (mTq) was attached to the 3' region of the native coding sequence, separated by a GSGSGS linker. A kanamycin resistance cassette was inserted before the gene for N-terminal tags or after the gene for C-terminal tags. When necessary, the promoter was duplicated. The

mutant was selected by plating on S6 agar plates supplemented with 50 µg/mL of kanamycin. All fusions were verified by PCR.

replaced with a spectinomycin resistance cassette, followed by a duplicated promoter for the downstream gene. Deletion of *Hn0716* was obtained by codon-optimizing the downstream gene and inserting the spectinomycin resistance cassette after this codon-optimized gene. Mutants were selected by plating on S6 agar plates supplemented with 50 µg/mL of spectinomycin. All mutations were verified by PCR.

Microscopy. All live-cell microscopy was performed using exponentially growing cells. 3-5 µL of cells were dropped onto a piece of 2% UltraPure agarose + S6 pad and imaged on a Mantek dish. All fluorescence and phase contrast imaging were performed using a Nikon Ti2-E motorized inverted microscope controlled by NIS Elements software with a SOLA 365 LED light source, a 100X Objective lens (Oil CFI Plan Apochromat DM Lambda Series for Phase Contrast), and a Photometrics Prime 95B Back-illuminated sCMOS camera or a Hamamatsu Orca Flash 4.0 LT + sCMOS camera. ParB-mNG, mNG-FliN, and CheY-mNG were imaged using a “GFP” filter set (C-FL GFP, Hard Coat, High Signal-to-Noise, Zero Shift, Excitation: 470/40 nm [450-490 nm], Emission: 525/50nm [500-550nm], Dichroic Mirror: 495 nm). CbbS-mTQ labeled carboxysomes were imaged using a “CFP” filter set (C-FL CFP, Hard Coat, High Signal-to-Noise, Zero Shift, Excitation: 436/20 nm [426-446 nm], Emission: 480/40 nm [460-500 nm], Dichroic Mirror: 455 nm). DAPI fluorescence was imaged using a standard “DAPI” filter set (C-FL DAPI, Hard Coat, High Signal-to-Noise, Zero Shift, Excitation: 350/50 nm [325-375 nm], Emission: 460/50 nm [435-485 nm], Dichroic Mirror: 400 nm). Alexa Fluor 594 C₅ maleimide-conjugated flagella were imaged using a “TexasRed” filter set (C-FL Texas Red, Hard Coat, High Signal-to-Noise, Zero Shift, Excitation: 560/40 nm [540-580 nm], Emission: 630/75 nm [593-668 nm], Dichroic Mirror: 585 nm).

Long-term microscopy. For multigenerational time-lapse microscopy, 1.5% UltraPure agarose + S6 pads were cast in a 35-mm glass-bottom dishes. Dishes were preincubated at 30°C in 5% CO₂ for at least 24 hr. 4 µL of exponentially growing cells were spotted onto the agar pad. Temperature, humidity, and CO₂ concentrations were controlled with a Tokai Hit Incubation System. NIS Elements software was used for image acquisition. Cells were preincubated in the stage top for at least 30 minutes before image acquisition. Videos were taken at one frame per 2.5-5 minutes for a duration of 12-24 hours.

Image analysis. Several fields of view were captured for each mutant. All fluorescence channels were subjected to background subtraction on Fiji with a rolling ball radius of 50 µm. Background-subtracted fluorescence images were merged with phase contrast images to create composites used for image analysis. Image analysis including cell identification, quantification of cell length, foci localization, foci number, foci fluorescence intensity, and identification of constriction sites were performed using Fiji plugin MicrobeJ 5.131 (Schindelin et al., 2012; Ducret et al., 2016). Cell perimeter detection and segmentation were done using the rod-shaped descriptor with default threshold settings at a tolerance of 56. Maxima detection parameters were individually set for each cargo. For ParB-mNG (cargo = chromosome) foci detection, tolerance and z-score were both set to 100. For CheY-mNG (cargo = chemotaxis) foci detection, tolerance was set to 150 and z-score was set to 100. For mNG-FliN (cargo = flagella) foci detection, tolerance was set to 710 and z-score was set to 69. For CbbS-mTq (cargo = carboxysome) foci detection, point detection was used instead of foci detection, and tolerance was set to 1010. Results were manually verified using the experiment editor, and non-segmented cells were cut using a particle cutter. Associations, shape descriptors, profiles, and localization were recorded for each strain. Localization graphs were automatically generated through MicrobeJ. Fluorescence intensity graphs and

foci number count graphs were made in GraphPad Prism (GraphPad Software, San Diego, CA, www.graphpad.com).

Nucleoid staining for live imaging. Cells were harvested by centrifugation at 5,000 g for 5 minutes. Following centrifugation, the cells were washed in PBS, pH 7.4. The resulting cell pellet was resuspended in 100 μ l PBS and stained with SytoxBlue at a final concentration of 500 nM. The samples were incubated in the dark, at room temperature for 5-10 minutes. Stained cells were directly loaded onto an S6 agar pad that had been infused with 500 nM SytoxBlue.

Carboxysome count. Eleven frames were captured over the course of 2 minutes. Carboxysomes were counted in each frame. The highest number counted per cell was used for carboxysome count.

Motility assay. Motility assays were run in S6 in 0.4% agar. Cells were grown on a plate of S6 medium. Individual colonies were inoculated into tubes or plates of motility media and incubated at 30°C. Tubes and plates were checked daily for motility for 2 weeks.

Cysteine-labelling of flagellin. *H. neapolitanus* flagellin was identified using a BLAST homology search with Hag from *Bacillus subtilis* as the query. Only a single flagellin gene was found. Several threonine and serine residues were considered for cysteine mutagenesis. Residues were mutated using the Q5 site-directed mutagenesis kit. Clones were verified for cysteine mutation by sequencing.

Flagella stain. Alexa Fluor 594 C₅ maleimide dye was resuspended in DMSO to the working concentration of 10 mM. *H. neapolitanus* cultures were grown to an OD of 0.1-0.2. The cultures were adjusted to a pH of 7.0 using PBS, pH 11.7. Cells at an adjusted pH of 7.0 were then stained with Alexa Fluor 594 C₅ maleimide dye at a final dye concentration of 100 μ M. Staining cultures were incubated overnight at 4°C. The stained cells were washed 4+ times in PBS, pH 7.4. All centrifugation steps were performed at 5,000xg for 3 minutes.

Statistical analysis. For all population analyses, we used a non-parametric Wilcoxon test using GraphPad Prism.

Complementation of mutants. Cells were grown to an OD of 0.1. They were induced with 0.25, 1, 5, 10, 50 μ M IPTG for up to 6 hours. They were imaged for complementation at various time points.

Divisome: gene encoding for *minD* was put under a pTrc promoter and induced with 50 μ M IPTG for 6 hours.

Carboxysome: gene encoding for *mcdAB* was put under a pTrc promoter and induced with 50 μ M IPTG for 3 hours.

Flagella: gene *Hn0716* was put under a pTrc promoter and was not induced with IPTG, saw complementation with leaky expression from the pTrc promoter

Chromosome: gene encoding for *parA* was put under the pTrc promoter and induced with 50 μ M IPTG for 3 hours.

Multiple cargo label construct. For the native fluorescent fusion of ParB-mScarlet, FliN-Halotag, and CheY-mNG, the sequence encoding for each respective fluorescent protein was attached to the 3' or 5' region of the native coding sequence, separated by a GSGSGS linker. For the native fluorescent fusion of Cbbs-mTQ, the sequence encoding mTurquoise (mTQ) was attached to the 3' region of the native coding sequence, separated by a GSGSGS linker.

Antibiotic cassettes were inserted before the gene for N-terminal tags or after the gene for C-terminal tags. The mutant was selected by plating on S6 agar plates supplemented with respective antibiotics. All fusions were verified by PCR. **Antibiotic cassettes:** For Cbbs-mTq, a kanamycin resistance cassette was inserted at the C-terminal and selected with 50 ug/mL kanamycin supplemented on S6 plates. For ParB-mScarlet, a chloramphenicol resistance cassette was inserted at the C-terminal of the gene and selected with 25 ug/mL Chloramphenicol supplemented on S6 plates. For FliN-Halotag, a tetracycline resistant cassette was inserted at the C-terminal of the gene and selected with 10 ug/mL tetracycline supplemented on S6 plates. For CheY-mNG, a carbenicillin resistance cassette was inserted at the C-terminal of the gene and selected with 10 ug/mL carbenicillin supplemented on S6 plates.

Halotag stain. JaneliaFluor650 far red dye was resuspended in DMSO to the working concentration of 5 uM. *H. neapolitanus* cultures were grown to an OD of 0.1-0.2. The cultures were washed with S6. Washed cells were then stained with JaneliaFluor650 dye at a final dye concentration of 200uM. Staining cultures were incubated for 3 hours at 37°C. The stained cells were washed 2 times with S6. All centrifugation steps were performed at 5,000xg for 5 minutes.

Bibliography

1. Alberts, B. *et al.* Molecular Motors. (2002).
2. Lutkenhaus, J. The ParA/MinD family puts things in their place. *Trends in Microbiology* vol. 20 411–418 (2012).
3. Vecchiarelli, A. G., Mizuuchi, K. & Funnell, B. E. Surfing biological surfaces: exploiting the nucleoid for partition and transport in bacteria. *Molecular Microbiology* **86**, 513–523 (2012).
4. Kiebusch, D. & Thanbichler, M. Spatiotemporal organization of microbial cells by protein concentration gradients. *Trends in Microbiology* **22**, 65–73 (2014).
5. Savage, D. F., Afonso, B., Chen, A. H. & Silver, P. A. Spatially Ordered Dynamics of the Bacterial Carbon Fixation Machinery. *Science (1979)* **327**, 1258–1261 (2010).
6. Maccready, J. S. & Vecchiarelli, A. G. Positioning the model bacterial organelle, the carboxysome. *mBio* **12**, (2021).
7. Rillema, R., MacCready, J. S. & Vecchiarelli, A. G. Cyanobacterial growth and morphology are influenced by carboxysome positioning and temperature. *bioRxiv* 2020.06.01.127845 (2020) doi:10.1101/2020.06.01.127845.
8. MacCready, J. S., Basalla, J. L. & Vecchiarelli, A. G. Origin and Evolution of Carboxysome Positioning Systems in Cyanobacteria. *Molecular Biology and Evolution* **37**, 1434–1451 (2020).
9. Hakim, P., Hoang, Y. & Vecchiarelli, A. G. Dissection of the ATPase active site of McdA reveals the sequential steps essential for carboxysome distribution. <https://doi.org/10.1091/mbc.E21-03-0151> **32**, ar11 (2021).
10. MacCready, J. S. *et al.* Protein gradients on the nucleoid position the carbon-fixing organelles of cyanobacteria. *Elife* **7**, (2018).
11. MacCready, J. S., Tran, L., Basalla, J. L., Hakim, P. & Vecchiarelli, A. G. The McdAB system positions α -carboxysomes in proteobacteria. *Molecular Microbiology* **00**, 1–21 (2021).
12. Campos-García, J., Nájera, R., Camarena, L. & Soberón-Chávez, G. The *Pseudomonas aeruginosa* motR gene involved in regulation of bacterial motility. *FEMS Microbiology Letters* **184**, 57–62 (2000).
13. Blagotinsek, V. *et al.* An ATP-dependent partner switch links flagellar C-ring assembly with gene expression. *Proceedings of the National Academy of Sciences* **117**, 20826–20835 (2020).
14. Kusumoto, A. *et al.* Regulation of polar flagellar number by the flhF and flhG genes in *Vibrio alginolyticus*. *Journal of Biochemistry* **139**, 113–121 (2006).
15. Schuhmacher, J. S. *et al.* MinD-like ATPase FlhG effects location and number of bacterial flagella during C-ring assembly. *Proc Natl Acad Sci U S A* **112**, 3092–3097 (2015).
16. Schuhmacher, J. S., Thormann, K. M. & Bange, G. How bacteria maintain location and number of flagella? *FEMS Microbiology Reviews* **39**, 812–822 (2015).
17. Thompson, S. R., Wadhams, G. H. & Armitage, J. P. The positioning of cytoplasmic protein clusters in bacteria. *Proc Natl Acad Sci U S A* **103**, 8209–8214 (2006).
18. Jones, C. W. & Armitage, J. P. Positioning of bacterial chemoreceptors. *Trends in Microbiology* **23**, 247–256 (2015).
19. Ringgaard, S., Schirner, K., Davis, B. M. & Waldor, M. K. A family of ParA-like ATPases promotes cell pole maturation by facilitating polar localization of chemotaxis proteins. *Genes Dev* **25**, 1544–1555 (2011).
20. Ringgaard, S. *et al.* ParP prevents dissociation of CheA from chemotactic signaling arrays and tethers them to a polar anchor. *Proc Natl Acad Sci U S A* **111**, (2014).
21. Leipe, D. D., Wolf, Y. I., Koonin, E. v. & Aravind, L. Classification and evolution of P-loop GTPases and related ATPases. *Journal of Molecular Biology* **317**, 41–72 (2002).

22. Baxter, J. C. & Funnell, B. E. Plasmid Partition Mechanisms. *Microbiology Spectrum* **2**, (2014).
23. Jalal, A. S. B. & Le, T. B. K. Bacterial chromosome segregation by the ParABS system. *Open Biology* **10**, 200097 (2020).
24. Atmakuri, K., Cascales, E., Burton, O. T., Banta, L. M. & Christie, P. J. Agrobacterium ParA/MinD-like VirC1 spatially coordinates early conjugative DNA transfer reactions. *EMBO J* **26**, 2540–2551 (2007).
25. Livny, J., Yamaichi, Y. & Waldor, M. K. Distribution of centromere-like parS sites in bacteria: Insights from comparative genomics. *Journal of Bacteriology* **189**, 8693–8703 (2007).
26. Yu, X. & Margolin, W. FtsZ ring clusters in min and partition mutants: role of both the Min system and the nucleoid in regulating FtsZ ring localization. *Mol Microbiol* **32**, 315–326 (1999).
27. Axen, S. D., Erbilgin, O. & Kerfeld, C. A. A Taxonomy of Bacterial Microcompartment Loci Constructed by a Novel Scoring Method. *PLoS Computational Biology* **10**, e1003898 (2014).
28. Turmo, A., Gonzalez-Esquer, C. R. & Kerfeld, C. A. Carboxysomes: metabolic modules for CO₂ fixation. *FEMS Microbiology Letters* **364**, (2017).
29. MacCready, J. S., Tran, L., Basalla, J. L., Hakim, P. & Vecchiarelli, A. G. The McdAB system positions α -carboxysomes in proteobacteria. *Molecular Microbiology* **00**, 1–21 (2021).
30. Mears, P. J., Koirala, S., Rao, C. v., Golding, I. & Chemla, Y. R. Escherichia coli swimming is robust against variations in flagellar number. *Elife* **2014**, (2014).
31. Huitema, E., Pritchard, S., Matteson, D., Radhakrishnan, S. K. & Viollier, P. H. Bacterial Birth Scar Proteins Mark Future Flagellum Assembly Site. *Cell* **124**, 1025–1037 (2006).
32. Lam, H., Schofield, W. B. & Jacobs-Wagner, C. A Landmark Protein Essential for Establishing and Perpetuating the Polarity of a Bacterial Cell. *Cell* **124**, 1011–1023 (2006).
33. Koonin, E. v. A Superfamily of ATPases with Diverse Functions Containing Either Classical or Deviant ATP-binding Motif. *J Mol Biol* **229**, 1165–1174 (1993).
34. Dasgupta, N., Arora, S. K. & Ramphal, R. fleN, a gene that regulates flagellar number in Pseudomonas aeruginosa. *Journal of Bacteriology* **182**, 357–364 (2000).
35. Amsterdam, K. van & Ende, A. van der. Helicobacter pylori HP1034 (ylxH) is required for motility. *Helicobacter* **9**, 387–395 (2004).
36. Chang, Y. *et al.* Molecular mechanism for rotational switching of the bacterial flagellar motor. *Nature Structural & Molecular Biology* **27**:11 **27**, 1041–1047 (2020).
37. Thiem, S. & Sourjik, V. Stochastic assembly of chemoreceptor clusters in Escherichia coli. *Molecular Microbiology* **68**, 1228–1236 (2008).
38. Alley, M. R., Maddock, J. R. & Shapiro, L. Polar localization of a bacterial chemoreceptor. *Genes & Development* **6**, 825–836 (1992).
39. Roberts, M. A. J., Wadhams, G. H., Hadfield, K. A., Tickner, S. & Armitage, J. P. ParA-like protein uses nonspecific chromosomal DNA binding to partition protein complexes. *Proc Natl Acad Sci U S A* **109**, 6698–6703 (2012).
40. Kentner, D. & Sourjik, V. Dynamic map of protein interactions in the Escherichia coli chemotaxis pathway. *Molecular Systems Biology* **5**, 238 (2009).
41. Sourjik, V. & Berg, H. C. Localization of components of the chemotaxis machinery of Escherichia coli using fluorescent protein fusions. *Molecular Microbiology* **37**, 740–751 (2000).
42. Briegel, A. *et al.* Universal architecture of bacterial chemoreceptor arrays. *Proceedings of the National Academy of Sciences* **106**, 17181–17186 (2009).
43. Bindels, D. S. *et al.* MScarlet: A bright monomeric red fluorescent protein for cellular imaging. *Nature Methods* **14**, 53–56 (2016).
44. Schumacher, M. A. *et al.* Structural Mechanism of ATP-induced Polymerization of the Partition Factor ParF. *J Biol Chem* **287**, 26146–26154 (2012).

45. Radnedge, L., Youngren, B., Davis, M. A. & Austin, S. Probing the structure of complex macromolecular interactions by homolog specificity scanning: the P1 and P7 plasmid partition systems. *EMBO J* **17**, 6076–6085 (1998).
46. Ravin, N. v, Rech, J. & Lane, D. Mapping of Functional Domains in F Plasmid Partition Proteins Reveals a Bipartite SopB-recognition Domain in SopA. *J Mol Biol* **329**, 875–889 (2003).
47. Barilla, D., Carmelo, E. & Hayes, F. The tail of the ParG DNA segregation protein remodels ParF polymers and enhances ATP hydrolysis via an arginine finger-like motif. *Proc Natl Acad Sci USA* **104**, 1811–1816 (2007).